Available online at www.sciencedirect.com
ScienceDirect
Journal of Power Sources 175 (2008) 874–880
JOURNAL OF POWER SOURCES
www.elsevier.com/locate/jpowsour

Sb-coated mesophase graphite powder as anode material for lithium-ion batteries

Chia-Chin Chang *

Department of Environment and Energy, National University of Tainan, Tainan 701, Taiwan

Received 16 March 2007; received in revised form 21 September 2007; accepted 25 September 2007
Available online 10 October 2007

Abstract

Antimony-coated mesophase graphite powder (MGP) composites are developed as an alternate anode material for Li-ion batteries using an argon atmosphere pyrolysis technique. The specific discharge capacity and cycle life of the Sb-MGP composites are studied. The Sb loading of the Sb-MGP has a significant effect on the composite performance. The Sb-MGP samples demonstrate improved lithium storage capacity. The Sb loading on MGP is optimized experimentally to obtain the maximum reversible capacity for composite electrodes. The reaction processes of lithium intercalation/de-intercalation in MGP and alloying of lithium/Sb are identified by cyclic voltammetry. ICP and EDS measurements confirm the presence of Sb in the MGP matrix. Differential scanning calorimetry (DSC) scans of lithium intercalated anodes show that Sb loading on the MGP material reduces the thermal stability of the anode.

Keywords: Lithium-ion battery; Sb; Antimony; Mesophase graphite powder; MGP; Pyrolysis

1. Introduction

Graphite- or coke-based carbon materials are widely used as anodes in commercial lithium-ion batteries due to low potential plateau, acceptable capacity, stable cycling performance and low cost. However, some electrochemical properties (e.g. energy density, capacity, etc.) of carbon anodes are insufficient for market needs. In order to increase the specific energy of lithium-ion batteries, new anode materials such as lithium alloys [1,2], tin oxides and tin alloys [3–7], silicon and its compounds [8,9], Mg_2Ge [10], $Li_{2.6}Co_{0.4}N$ [11,12] and $CoSb_3$ [13] have been studied. Compared with carbonaceous materials, Sn-, Si- and Sb-based composite oxides and alloys show higher specific capacity as anode active materials [14,15]. However, most composite oxides and alloy anode materials exhibit rather large capacity loss at the first charge/discharge cycle as well as fading capacity during cycling. These phenomena originate from the following factors: decomposition of the surface oxide [7]; formation of a solid electrolyte interphase on the surface of the material [16]; irreversible trapping of Li ions by host atoms [7]; serious aggregation of metal particles during electrochemical cycling [7]; large volume change [17]. Various works have shown that problems of volume change and metal particle aggregation can be alleviated significantly by use of superfine intermetallic compounds and active/inactive composite alloy materials, thereby providing large capacities with acceptable irreversible capacity in the first cycle, although cycle life remains problematical [2,5,18,19]. Metal-based carbon composites such as metallic Sn [20–23], Sn oxides [17,24–27], Sn alloys [28,30], Sb alloys [31] and Si [32–34] have shown promise in overcoming first-cycle capacity loss and multi-cycle capacity fade, although problems continue related to either capacity or cyclability. Chemical and electrochemical stability are also difficult to control in these systems. Electrochemical performance of the composites is influenced by the kinds of metals, particle size distribution of the metal compounds and the amount of metal on the material surface.

Combing the high capacity of Sb with the good cycling behavior of carbon has yielded interesting results. With this approach, Santos-Peňa et al. [32] used pyrolysis of tin chlorides with graphite in Ar atmosphere to synthesize Sn–C composites, showing that first-cycle irreversible capacity loss was reduced with suitable amounts of Sn in the graphite. Our group previously reported an economical and efficient pyrolysis technique

* Tel.: +886 62606123x7208; fax: +886 62602205.
E-mail address: ccchang@mail.nutn.edu.tw.

0378-7753/$ – see front matter © 2007 Elsevier B.V. All rights reserved.
doi:10.1016/j.jpowsour.2007.09.108

for loading fine amorphous particles of modified metals onto substrates such as titanium and graphite [35]. This present study explores improvement of graphite composite anodes for Li-ion batteries by pyrolysis of Sb onto mesophase graphite powder (MGP). In the following, Sb loading on graphite is studied and optimized experimentally to obtain the maximum reversible discharge capacity. Differential scanning calorimetry (DSC) and electrochemical characterization are performed to evaluate the Sb–C composite as a Li-ion anode material.

2. Experimental

2.1. Preparation of Sb-MGP composite anodes

The mesophase graphite powders (MGP, China Steel Chemical Co., Taiwan) used in this work had an average particle size of 24.3 μm and a Brunauer–Emmett–Teller (BET) surface area of 0.52 $m^2\,g^{-1}$. Our preparation of Sb-coated MGP material began with dissolving $SbCl_3$ into an isopropanol solution containing 30% by volume concentrated HCl. Suitable amounts of Sb yielded 0.167, 0.5, 1.0, 1.5 and 2.0 mol dm^{-3} total solutions. Next, 60 g of MGP power was added to 540 ml of each of the above $SbCl_3$ solutions and then stirred magnetically for more than 24 h. To remove the solvent, the mixture was heated at 100 °C in an oven under continuous stirring. After about 6 h, the solvent was gone and the material had aggregated into a granular solid. The aggregated blend then was heated in a furnace for 2 h at 450 °C under Ar atmosphere to induce pyrolysis, after which the furnace was cooled to room temperature, still under Ar ambient. The obtained Sb-MGP composite sample was finally hand-milled in a mortar and sieved at a pore size of 200 μm mesh.

Electrodes were prepared by mixing Super S (1.53 wt%, MMM Carbon, Belgium), polyvinylidenedifluoride powder (3.57 wt%, PVDF W1300, Kureha Chemical Industry, Japan) and Sb-MGP composite (94.9 wt%) in *N*-methylpyrolidinone (NMP, ISP Corp., USA) solvent. The mixed slurry was then coated onto copper foil (10 μm, Nippon Foil Co., Japan) and dried at 90 °C. The dried electrode was compressed by a roller at room temperature to make a smooth and compact film structure. The composite anode electrode was stored in a glove box with oxygen and humidity content maintained below 5 ppm for more than 24 h before electrochemical characterization. In total, six electrodes were prepared, one pristine MGP and the others as 0.167, 0.5, 1.0, 1.5 and 2.0 mol dm^{-3} $SbCl_3$-treatments of the MGP surface.

2.2. Electrochemical characteristics testing

Electrochemical performance of the Sb-MGP composite anodes was examined by use of two-electrode test cells (coin-type cells) which consisted of a composite electrode, a microporous separator (Celgard 2300), a metallic lithium electrode and an electrolyte of 1 mol dm^{-3} $LiPF_6$ in a weight ratio 1:1 mixture of ethylene carbonate (EC) and diethyl carbonate (DEC). Coin-type cells for testing were assembled in a glove box. Lithium sheet (FMC) of 0.02 mm thickness was cut into disk shapes for use as negative electrodes. Test cells were tested for charge/discharge behavior in a constant current mode, cycled galvanostatically at 0.325 mA cm^{-2} over the range of 0.01–2.0 V. Cyclic voltammetry (CV) measurements were conducted with an Autolab electrochemical analyzer (Autolab PGSTAT30, Eco Chemie) with a current sensitivity of 1 nA. A one-compartment three-electrode polypropylene cell was used and the whole apparatus was set in a glove box. The working electrode was one of the Sn-MGP composite electrodes prepared by the above procedure, with a dimension of 1 cm × 1 cm. Both the counter and reference electrodes were lithium metal. The electrolyte was 1 mol dm^{-3} $LiPF_6$ dissolved in weight ratio 1:1 of EC and DEC solvents.

2.3. Material characteristics testing

Antimony content of the MGP composites was determined by inductively coupled plasma spectroscopy (ICP, Optima 2000 DV, Perkin-Elmer) using composite samples digested in a HCl/HNO_3 mixture, respectively, 1:3 by volume. Surface morphology and surface composition of the composite electrodes were evaluated by scanning electron microscopy (SEM, Jeol JSM35, operating at 20 kV) and energy dispersive spectroscopy (EDS). Sb-MGP specimens were inspected microscopically and spectroscopically soon after preparation and prior to electrochemical testing.

Differential scanning calorimetry (DSC) experiments were conducted after charging the electrodes to 0.0 V at 0.325 mA cm^{-2} using a DSC Perkin-Elmer calorimeter. Using a glove box, approximately 4 mg of the anode composite containing the electrolyte were hermetically sealed in an aluminum DSC pan. The samples were analyzed in the DSC at a temperature scan rate of 10 °C per min from 40 to 300 °C.

3. Results and discussion

SEM observation was performed to characterize the morphologies of the MGP and the Sb-MGP composite materials. Fig. 1 shows SEM images of the pristine MGP and the various Sb-MGP composites. The pristine MGP, Fig. 1(a), is seen to have a distinctly spherical shape. In Fig. 1(b), Sb loading is indicated by bright spots on the spherical MGP surface. With increasing Sb loading across the sequence of Fig. 1(b)–(f), the white spots expand over the MGP surface and then begin to form larger crystals which exhibit the angular rhombohedral structure expected of antimony. This clearly indicates that Sb is loading onto the MGP surface through pyrolytic modification. Fig. 2 shows EDS analysis of the pristine MGP and the Sb-MGP modified by the 0.5 mol dm^{-3} $SbCl_3$ solution. The Sb-MGP plot clearly shows the appearance of Sb and oxygen peaks which are not present for the pristine MGP, confirming the presence of Sb and oxygen. The Sb content of the prepared MGP samples as analyzed by inductively coupled plasma spectroscopy is given in Table 1.

The influence of the amount of Sb on the electrochemical properties of the Sb-MGP composite was studied by cyclic voltammetry (CV). The first and second cycles of the CV plots

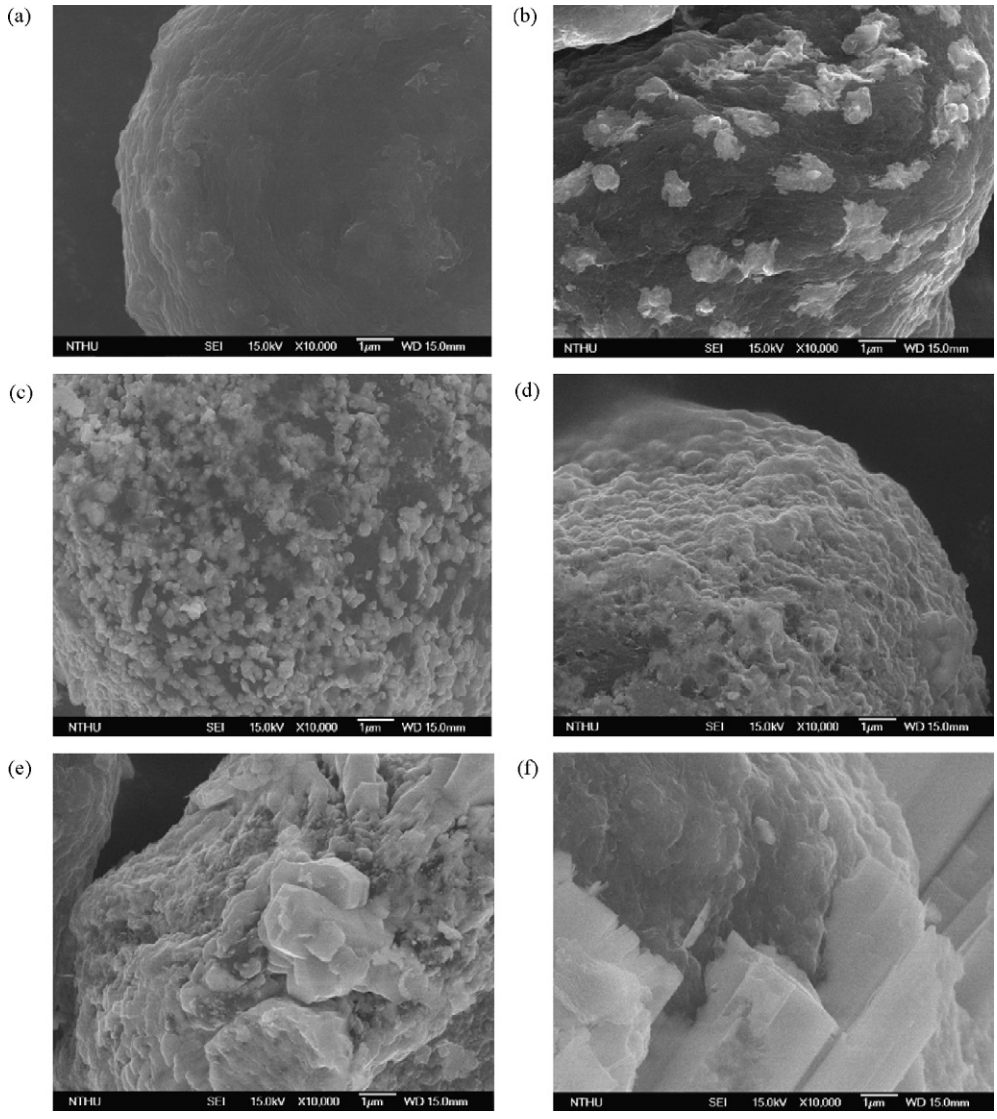

Fig. 1. SEM micrographs at 10,000× magnification of pristine MGP and Sb-MGP composite anodes: (a) pristine MGP, (b) 0.85 wt%, (c) 2.41 wt%, (d) 3.07 wt%, (e) 3.70 wt%, (f) 4.72 wt%.

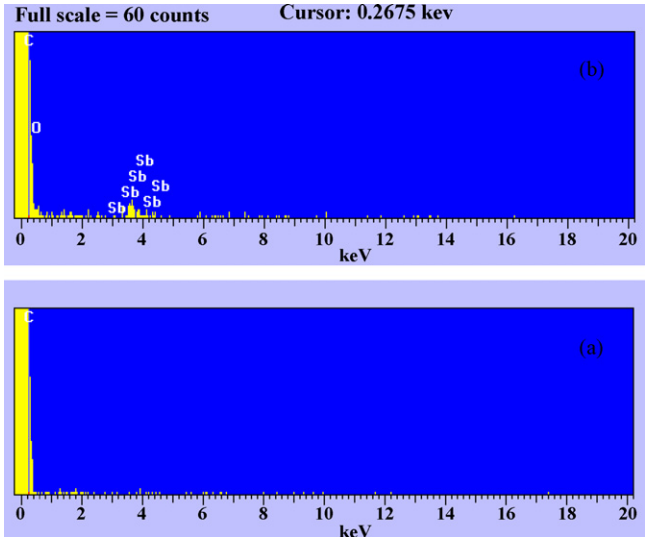

Fig. 2. EDS of (a) pristine MGP and (b) 2.41 wt% Sb-MGP composite.

Table 1
$SbCl_3$ concentration of modification solution and actual amount of Sb loading on MGP for preparation at 60 g MGP, 540 ml $SbCl_3$ solution

Sample	$SbCl_3$ concentration in isopropanol solution (mol dm^{-3})	wt% of Sb on Sb-MGP
a	–	0
b	0.167	0.85
c	0.5	2.41
d	1.0	3.07
e	1.5	3.70
f	2.0	4.72

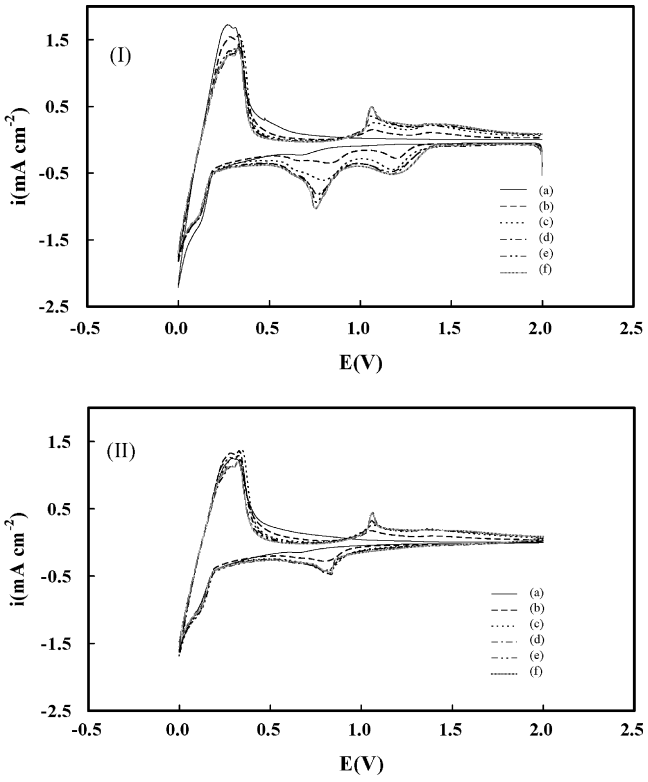

Fig. 3. Cyclic voltammograms from (I) the 1st scan and (II) the 2nd scan at 0.1 mV s^{-1} in 1 mol dm^{-3} $LiPF_6$ EC–DEC (1:1 by weight) electrolyte at pristine MGP and Sb-MGP composite anodes: (a) pristine MGP, (b) 0.85 wt%, (c) 2.41 wt%, (d) 3.07 wt%, (e) 3.70 wt%, (f) 4.72 wt%. Potential range is 2.0–0.0 V.

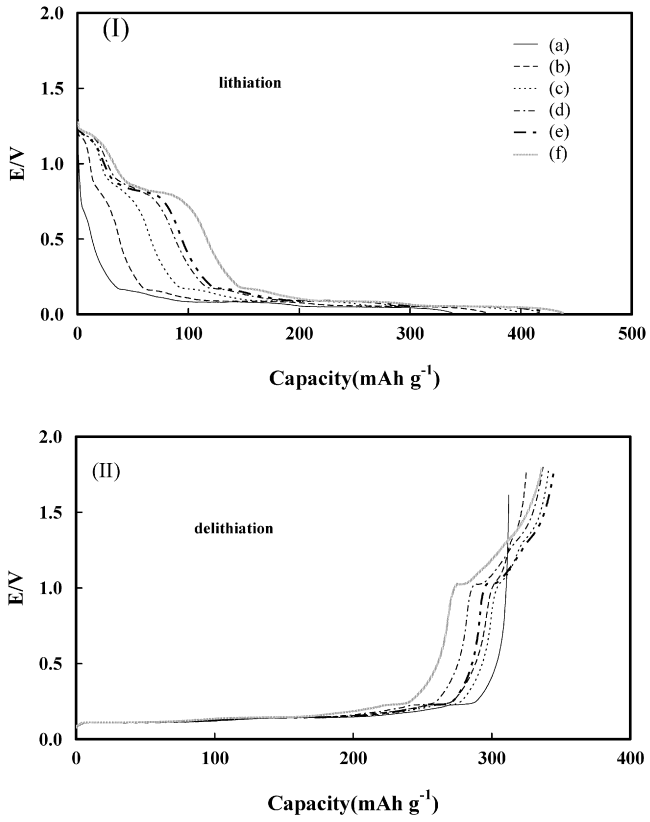

Fig. 4. The first cycle (I) lithiation and (II) delithiation of pristine MGP and Sb-MGP composite anodes: (a) pristine MGP, (b) 0.85 wt%, (c) 2.41 wt%, (d) 3.07 wt%, (e) 3.70 wt%, (f) 4.72 wt%. Current density is 0.325 mA cm^{-2} at a potential range of 0.01–2.0 V.

for the Sb-MGP composite electrodes in 1 mol dm^{-3} $LiPF_6$ EC–DEC solution at a scan rate of 0.1 mV s^{-1} are shown in Fig. 3(I) and (II), respectively. During the first reduction (Fig. 3(I)), three peaks are observed at 1.25, 0.75 and 0 V versus Li^+/Li. However, in the following cycle (Fig. 3(II)) the 1.25 V peak has disappeared, a phenomenon that can be attributed to the irreversible reduction of antimony oxides. The reactions occurring between 1.5 and 1.0 V correspond to the formation of lithium oxide and metallic antimony [36]. The peak currents increase slightly with increasing wt% of Sb on the Sb-MGP, which may be related to the amount of surface antimony oxide on the antimony particles. The broad and intense peak starting around 0.90 V and centered around 0.75 V presumably corresponds to the formation of a passivation film [37] and, simultaneously, to the insertion of lithium into antimony with the formation of lithium–antimony alloys (as Li_2Sb at 0.859 V and Li_3Sb at 0.813 V) [36,37]. The peak currents increase significantly with increasing wt% of Sb on the Sb-MGP composite. This behavior agrees with the SEM results, i.e. the size of the antimony particles increases with increasing quantity of antimony on the Sb-MGP surface. The lithium de-intercalation currents between 0.35 and 0.90 V sequentially decrease with increasing antimony. This result indicates that antimony on the MGP surface influences the Li-graphite de-intercalation behavior. The broad peak of the oxidation current between 0.9 and 2.0 V corresponds to the de-insertion of lithium from lithium antimony alloys.

Fig. 4 shows the (I) Li-insertion and (II) Li-extraction curves of the MGP/Li and Sb-MGP/Li cells at 0.325 mA cm^{-2} over the potential range between 0.01 and 2.0 V. The Li-insertion curves (Fig. 4(I)) can be divided into three parts: a shoulder at 1.20 V, a pseudo-plateau near 0.8 V and a succession of plateaus for potential lower than 0.2 V. The first shoulder of the Li-insertion curves at ca. 1.20 V shows the reduction of antimony oxides by lithium with the subsequent formation of Li_2O and metallic antimony [37]. The 1.20 V plateau increases with increasing antimony wt% on the Sb-MGP composite surface. The formation of Li_2O and metallic antimony appear as an irreversible reaction that contributes partly to the irreversibility of this system. During Li insertion, Li–Sb alloys are formed in the voltage range of 0.9–0.2 V [37,38] while intercalation of Li ions into the interlayers of the MGP crystal lattice occurs mainly below 0.2 V. The 0.8 V plateau (Fig. 4(I)) increases significantly as the wt% of Sb increases, which shows that the amount of Li–Sb alloy increases with increasing Sb. In contrast, the Li-extraction process appears to result from a two-phase reaction. Lithium desertions in the graphite occur over the potential between 0.01 and 0.2 V. Decomposition of lithium–antimony alloys is marked by a shoulder near 1.0 V (Fig. 4(II)), which also increases with increasing Sb wt%. Significantly, the alloy reactions and the intercalation reactions are reversible. The reversible capacity for the Sb-MGP of sample (e) is as high as 345 mAh g^{-1}. The voltage profiles for all the Sb-MGP samples are similar but the

Table 2
Electrochemical performance of pristine MGP and Sb-MGP composites

	Pristine (a)	wt% of Sb on Sb-MGP				
		(b) (0.85%)	(c) (2.41%)	(d) (3.07%)	(e) (3.70%)	(f) (4.72%)
First Li-insertion capacity (mAh g^{-1})	338	369	398	413	422	437
First Li-extraction capacity (mAh g^{-1})	312	325	341	337	345	336
Coulombic efficiency at the first cycle (%)	92.31	88.08	85.68	81.60	81.76	76.89
Ratio of 20th Li-extraction capacity relative to 1st Li-extraction capacity (mAh g^{-1})	73.40	101.23	87.39	87.24	75.65	62.50

capacity ratio of the alloy reaction versus the Li intercalation reaction differs depending on the Sb wt%.

Table 2 shows the electrochemical performance of pristine MGP and Sb-MGP composite electrodes for the coin cell tests. The increase in the first-cycle Li-extraction capacity due to Sb addition is immediately obvious, although this was achieved with some loss of cyclability at high Sb content. Comparing the pristine MGP and Sb-MGP composite electrodes, the irreversible capacity of the alloy reaction (Li–Sb) for the Sb-MGP composite increases with increasing Sb wt%. The coulombic efficiency at first cycle for the pristine MGP and the Sb-MGP composite electrodes decreases with increasing Sb from 92.31% to 76.89%. These Sb-MGP values are lower than the pristine MGP material, which may be the result of Sb oxides reacting with Li^+ [38] and/or the presence of a solid electrolyte interphase (SEI) layer on the surface of the Sb particles during discharge/charge [39], as observed above in the CV studies. The first-cycle Li-insertion curve is marked by a pseudo-plateau near 0.8 V. This suggests a mechanism related to formation both of a passivation layer and also lithium–antimony alloy, especially since it is known that SEI films form on both carbon materials and on lithium storage metals [39]. The size of the Sb particles is larger for the Sb-MGP with higher Sb wt%. The larger Sb particles can then dissociate to smaller particles and thus increase the surface area of the particles. Surface filming consumes lithium and thus increases the irreversible capacity.

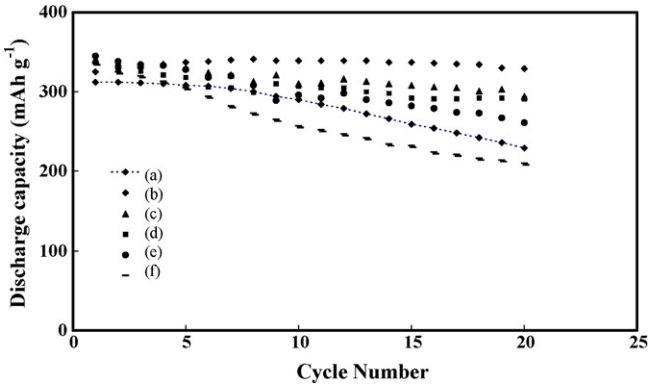

Fig. 5. The discharge capacity vs. cycle number of pristine MGP and Sb-MGP composite anodes: (a) pristine MGP, (b) 0.85 wt%, (c) 2.41 wt%, (d) 3.07 wt%, (e) 3.70 wt%, (f) 4.72 wt%. Charge and discharge current density is 0.325 mA cm^{-2} at a potential range of 0.01–2.0 V.

Fig. 5 shows the cycling characteristic of the pristine MGP and Sb-MGP anodes over 20 cycles at 0.325 mA cm^{-2} between 0.01 and 2.0 V. Examination of Fig. 5 reveals that the cycle performance of the sample (b) Sb-MGP composite (101.25% for 20 cycles) is better than the other samples. The cycle performance results of the Sb-MGP composites show a higher specific capacity as compared with the pristine MGP due to the presence of antimony, but the capacity fade increases with increasing Sb wt%. When compared to other published Sb-graphite or

Table 3
Comparison of the capacity of the Sb composite anode materials

Material	Cycling range (V)	Initial discharge extraction capacity (mAh g^{-1})	Irreversible capacity ratio (%)	Capacity retained at cycle[a] (%)				Reference
				10	20	30	40	
Sb-MGP	2.0–0.01	325	11	101.5	101.23			This work
Sb-graphite	2.0–0	400	50	105	105	105		[37]
SbSn-MCMB (Sn:9.7%, Sb:16.4%)	2.0–0	400	23.1	80	78			[39]
Sb-graphite	2.0–0	500[b]	26.5[b]			88[b]	84[b]	[41]
$SnSb_x$/carbonaceous mesophase spherules	1.5–0	431	20.5	92.1	91.6	90.5		[28]
$SnSb_x$/graphite	1.5–0	296	43.1	69.3	67.6	55.7		[28]
$SnSb_{0.13}$	0.8–0	540	37.2	96.3	85.2	74.1		[38]
$CoSb_2$	2.0–0	580	39	86.2	70.7			[42]
Zn_4Sb_3/C_7	2.5–0	625	39	64				[15]
Ag_3Sb	1.2–0	680	27.3	61.8	56.6	48.5	42.6	[43]
Cu_2Sb	1.2–0	320	34.7	92.2	91.9			[44]

[a] Capacity retention based on 1st cycle discharge capacity.
[b] Capacity retention based on 20th cycle discharge capacity.

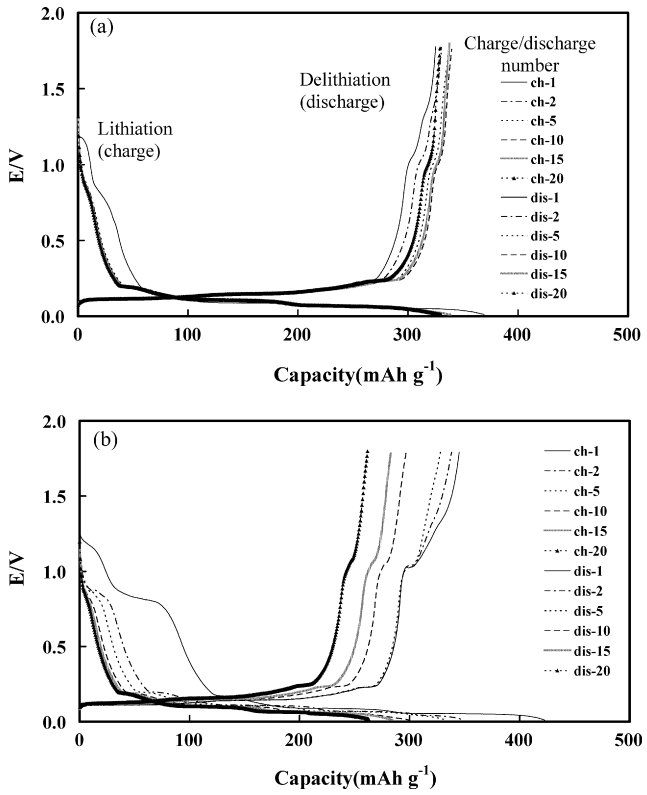

Fig. 6. The lithiation/delithiation curves of Sb-MGP composites anode in a lithium battery: (a) 0.85 wt% and (b) 4.72 wt%. Current density is 0.325 mA cm^{-2}. Electrolyte is 1 mol dm^{-3} $LiPF_6$ EC–DEC (1:1 by weight).

Sb alloys graphite composites (Table 3) this study's 0.85 wt% Sb-MGP composite anode shows superior capacity fade characteristics. This result is similar to Dailly et al. [40], who reported that Sb–carbon composite prepared by reduction of $SbCl_5$ by KC8 in tetrahydrofuran demonstrated reduced capacity fade.

Fig. 6 illustrates the lithiation (charge) and delithiation (discharge) curves between 0.01 and 2.0 V at 0.325 mA cm^{-2} of two prepared composite anodes: (a) 0.85 wt% Sb-MGP and (b) 4.71 wt% Sb-MGP. In each profile, a multi-plateau voltage region appears around 0.2–0.8 V (vs. Li/Li^+) which indicates the insertion/extraction of lithium in the Sb particles. During cycling, antimony shows similar working voltages near 0.8 V for Li^+-insertion and near 1.0 V for Li^+-release. The corresponding electrode reaction is connected to the reversible formation of Li_3Sb at about 0.8 V and its further decomposition at about 1.0 V. This interpretation is supported by the data given for intermetallic alloys like $SnSb_x$, Co_3Sb or pure antimony [1,37]. A long stable plateau around 0–0.2 V (vs. Li/Li^+) represents the insertion/extraction of lithium in MGP. Examination of Fig. 6(a) shows that the reaction corresponding to the high-voltage plateau of ~0.8 V for the 0.85 wt% Sb-MGP electrode is stable with increasing cycle number. As shown in Fig. 6(b), the 4.71 wt% Sb-MGP electrode exhibits a wide plateau at ~0.8 V during the first charge and discharge, after which the plateau length gets shorter and shorter with increasing cycle number. However, Li-extraction from graphite in the 0.01–0.2 V potential range is strongly influenced by the amount of Sb on the MGP surface during cycling. This can be attributed to dissociation of the large Sb particles into smaller particles and possible blocking of the graphite layer channels, resulting in worse cyclability. By comparison with pristine MGP, the cycling performances of Sb-MGP samples (b), (c) and (d) are significantly improved. Indeed, pristine graphite delivers a practical capacity of only 312 mAh g^{-1}. The presence of antimony in the composite gives an extra specific capacity of about 12 mAh g^{-1}. Moreover, the electrode appears stable upon cycling since for at least 20 cycles the Li-extraction capacity is stable at ca. 329 mAh g^{-1}. Also shown in Table 2 are the reversible specific capacities and the ratio of the capacity in the 20th cycle relative to the 1st cycle (R20/1), which can be used to indicate material endurance to repeated cyclic operation. There is an immediate increase in capacity after Sb addition, but that improvement is accompanied by some loss of cyclability at amounts of Sb higher than 0.85 wt%. Considering capacity and cyclability, this study finds the optimal weight ratio of Sb is ca. 0.85 wt% on the Sb-MGP composite surface, i.e. 0.167 mol dm^{-3} $SbCl_3$ 540 ml solution for 60 g MGP treatment.

By decomposition of metallic salts dissolved in organic solvents, a portion of the carbon may be deposited on the surface of MGP together with and/or encircling the metallic particles [29]. This may enhance the connection strength between the metallic particles and the carbon matrix. This may contribute to establishing and maintaining the distance between two metallic particles such that the inter-particle distance is long enough to prevent particle/particle contact after volume expansion, as in Fig. 1(b) (0.85 wt% Sb-MGP). Such a configuration seems able to reduce the mechanical stress caused by volume effects, improving the morphological and conducting stability of the Sb-MGP composites.

A DSC study was performed after charging the Sb-MGP composite anodes to 0.0 V to evaluate the effect of Sb loading on the thermal stability of the charged anodes. The thermal stability of pristine MGP and the Sb-MGP composite anodes are given in Fig. 7. The onset temperatures for thermal decomposition of pristine MGP and Sb-MGP composites are 130 and 100 °C, respectively. Examination of Fig. 7 shows that the exothermic peak temperature for pristine MGP is 140 °C. For the Sb-MGP composite anodes, this peak shifts to 135 °C and decreases further with increasing Sb. The total area of the exothermic peaks

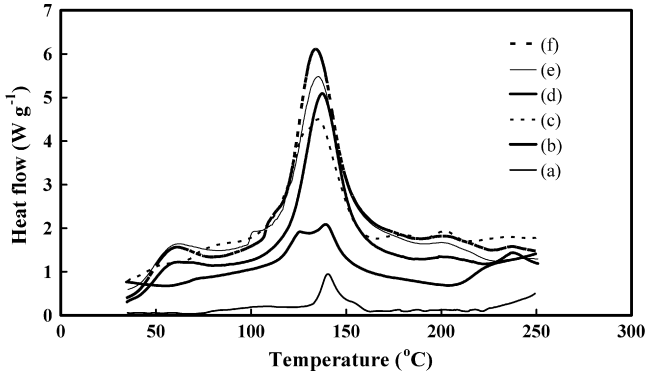

Fig. 7. DSC curves of lithiation anodes containing pristine MGP and Sb-MGP composite: (a) pristine MGP, (b) 0.85 wt%, (c) 2.41 wt%, (d) 3.07 wt%, (e) 3.70 wt%, (f) 4.72 wt%. Anode materials are charged to 0.0 V at 0.325 mA cm^{-2}.

of the Sb-MGP composites is greater than that of pristine MGP (13.15 J g^{-1}). The total exothermic peaks area of the Sb-MGP composites increases with increasing Sb wt%. These results for the onset temperature and the peak area of the first exothermic peak show that Sb coating on an MGP surface reduces the thermal stability of the anode in lithium-ion battery applications.

4. Conclusion

Composite materials in which Sb particles are modified onto the surface of carbon materials are prepared by an argon atmosphere pyrolytic technique. According to EDS and ICP-OES analysis of several MGP composites, it is probable that only a small amount of Sb has modified onto the graphite. The electrochemical properties of the Sb-MGP composites for Li-ion cells appear enhanced by the Sb modification treatment. The initial irreversible capacity and cyclic capacity fade of the Sb-MGP composite electrodes increase with increasing Sb loading. As a result, the cyclic performance of the composite materials is improved impressively, with a reversible capacity as high as 329 mAh g^{-1} after 20 cycles being obtained. Considering capacity and cyclic capability, the optimal weight ratio of Sb is ca. 0.85 wt% on the Sb-MGP composite surface, i.e. 0.167 mol dm^{-3} $SbCl_3$ 540 ml solution for 60 g MGP treatment. DSC results of charged anodes containing MGP and Sb-MGP composites show that Sb coating on the MGP surface may reduce the thermal stability of the anode. These studies will be extended to other quick and easy modification methods for graphite–metal systems in a quest for the best electrochemical performance for Li-ion batteries.

Acknowledgments

The author is grateful for the financial support of this work by China Steel Chemical Corporation, Taiwan, and the National Science Council of Taiwan under contract NSC 95-2221-E024-017, NSC 94-2623-7-024-001-ET and NSC 95-ET-7-024-001-ET. The author is also very much indebted to Mr. Yeong-Song Chen for assistance with the electrochemical measurements.

References

[1] R.A. Huggins, J. Power Sources 81–82 (1999) 13.
[2] J.O. Besenhard, J. Yang, M. Winter, J. Power Sources 68 (1997) 87.
[3] J. Read, D. Foster, J. Wolfenstine, W. Behl, J. Power Sources 96 (2001) 277.
[4] H. Li, L. Shi, W. Lu, X. Huang, L. Chen, J. Electrochem. Soc. 148 (2001) A915.
[5] Y. Idota, T. Kubota, A. Matsufuji, Y. Maekawa, T. Miyasaka, Science 276 (1997) 1395.
[6] W.H. Lee, H.C. Son, P.J. Reucroft, J.G. Lee, J.W. Park, J. Mater. Sci. Lett. 20 (2001) 39.
[7] H. Huang, E.M. Kelder, L. Chen, J. Schoonman, J. Power Sources 81–82 (1999) 362.
[8] B.A. Boukamp, G.C. Lesh, R.A. Huggins, J. Electrochem. Soc. 128 (1981) 725.
[9] R.A. Sharma, R.N. Seefurth, J. Electrochem. Soc. 123 (1976) 1763.
[10] H. Sakaguchi, H. Honda, T. Esaka, J. Power Sources 81–82 (1999) 229.
[11] M. Nishijima, T. Kagohashi, Y. Takeda, M. Imanishi, O. Yamamoto, J. Power Sources 68 (1997) 510.
[12] T. Shodai, Y. Sakurai, T. Suzuki, Solid State Ionics 122 (1999) 85.
[13] R. Alcántara, F.J. Fernándezmadrigal, P. Lavela, J.L. Tirado, J.C. Jumas, J. Oliverfourcade, J. Mater. Chem. 9 (1999) 2517.
[14] W. Xing, J.S. Xue, J.R. Dahn, J. Electrochem. Soc. 143 (1996) 3046.
[15] X.B. Zhao, G.S. Cao, Electrochim. Acta 46 (2001) 891.
[16] I.A. Courtney, J.R. Dahn, J. Electrochem. Soc. 144 (1997) 2045.
[17] J.Y. Lee, R. Zhang, Z. Liu, Electrochem. Solid State Lett. 3 (2000) 167.
[18] J. Yang, M. Wachtler, M. Winter, J.O. Besenhard, Electrochem. Solid State Lett. 2 (1999) 161.
[19] O. Mao, R.L. Turner, I.A. Courtney, B.D. Fredericksen, M.I. Buckett, L.J. Krause, J.R. Dahn, Electrochem. Solid State Lett. 2 (1999) 3.
[20] B. Veeraraghavan, A. Durairajan, B. Haran, B. Popov, R. Guidotti, J. Electrochem. Soc. 149 (2002) A675.
[21] G.X. Wang, J. Yao, H.K. Liu, S.X. Dou, J.H. Ahn, Electrochim. Acta 50 (2004) 517.
[22] T. Wang, J.Y. Lee, T.C. Deivaraj, J. Electrochem. Soc. 151 (2004) A1804.
[23] G.X. Wang, J. Yao, J.H. Ahn, H.K. Liu, S.X. Dou, J. Appl. Electrochem. 34 (2004) 187.
[24] Y. Wang, J.Y. Lee, B.H. Chen, Electrochem. Solid State Lett. 6 (2003) A19.
[25] J.Y. Lee, R. Zhang, Z. Liu, J. Power Sources 90 (2000) 70.
[26] R. Zhang, J.Y. Lee, Z.L. Liu, J. Power Sources 112 (2002) 596.
[27] Y. Wang, J.Y. Lee, J. Power Sources 144 (2005) 220.
[28] Y. Liu, J.Y. Xie, J. Yang, J. Power Sources 119–121 (2003) 572.
[29] Z.P. Guo, Z.W. Zhao, H.K. Liu, S.X. Dou, Carbon 43 (2005) 1392.
[30] X.Z. Liao, Z.F. Ma, J.H. Hu, Y.Z. Sun, X. Yuan, Electrochem. Commun. 5 (2003) 657.
[31] L. Aldon, A. Garcia, J. Olivier-Fourcads, J.C. Jumas, F.J. Fernández-Madrigal, P. Lavela, C.P. Vicente, J.L. Tirado, J. Power Sources 119–121 (2003) 585.
[32] J. Santos-Peňa, T. Brousse, D.M. Schleich, Solid State Ionics 135 (2000) 87.
[33] N. Dimov, S. Kugino, M. Yoshio, Electrochim. Acta 48 (2003) 1579.
[34] M. Yoshio, H. Wang, K. Fukuda, T. Umeno, N. Dimov, Z. Dgumi, J. Electrochem. Soc. 149 (2002) A1598.
[35] C.C. Chang, T.C. Wen, Mater. Chem. Phys. 47 (1997) 203.
[36] X.B. Zhao, G.S. Cao, C.P. Lv, L.J. Zhang, S.H. Hu, T.J. Zhu, B.C. Zhou, J. Alloy Compd. 315 (2001) 265.
[37] A. Dailly, J. Ghanbaja, P. Willmann, D. Billaud, Electrochim. Acta 48 (2003) 977.
[38] J. Yang, Y. Takeda, N. Imanishi, T. Ichikawa, O. Yamamoto, Solid State Ionics 135 (2000) 175.
[39] L. Shi, H. Li, Z. Wang, X. Huang, L. Chen, J. Mater. Chem. 11 (2001) 1502.
[40] A. Dailly, L. Balan, J. Ghanbaja, P. Willmann, D. Billaud, Carbon 43 (2005) 1001.
[41] A. Dailly, J. Ghanbaja, P. Willmann, D. Billaud, J. Power Sources 136 (2004) 281.
[42] J. Xie, G.S. Cao, X.B. Zhao, Y.D. Zhang, M.J. Zhao, J. Electrochem. Soc. 151 (2004) A1905.
[43] J.T. Vaughey, L. Fransson, H.A. Swinger, K. Edström, M.M. Thackeray, J. Power Sources 119–121 (2003) 64.
[44] L.M.L. Fransson, J.T. Vaughey, R. Benedek, K. Edström, J.O. Thomas, M.M. Thackeray, Electrochem. Commun. 3 (2001) 317.